Gas Phase Reactions

Heating: **furnace, laser, plasma, flame, arc**

Gas-Metal Rxn

$Ti + N_2 \xrightarrow{1800\ K} TiN$

$3\ Si + 2\ N_2 \longrightarrow Si_3N_4$

$W + CH_4 \longrightarrow WC + H_2$ **mp 2720 °C**

WC dissolved in Co = cemented carbides

$Ti + CH_4 \longrightarrow TiC + H_2$ **mp 2940 °C**

cementite

$steel + H_2/CO + CH_4 + NH_3 \longrightarrow Fe_3C + nitrides$

Gas Phase Reactions

Gas-Gas Rxn

homogeneous nucleation from supersaturated vapor (nano)

Flame hydrolysis
volatile compounds are passed through an oxygen-hydrogen stationary flame:

$$SiCl_4 + H_2 + O_2 \longrightarrow SiO_2 + HCl$$ **fumed silica**

reagent	bp/°C	product
$SiCl_4$	57	SiO_2
$AlCl_3$	180 (subl.)	Al_2O_3
$TiCl_4$	137	TiO_2
CrO_2Cl_2	117	Cr_2O_3
$Fe(CO)_5$	103	Fe_2O_3
$GeCl_4$	84	GeO_2
$Ni(CO)_4$	42	NiO
$SnCl_4$	114	SnO_2
$ZrCl_4$	331 (subl.)	ZrO_2
$VOCl_3$	127	V_2O_5

Gas Phase Reactions

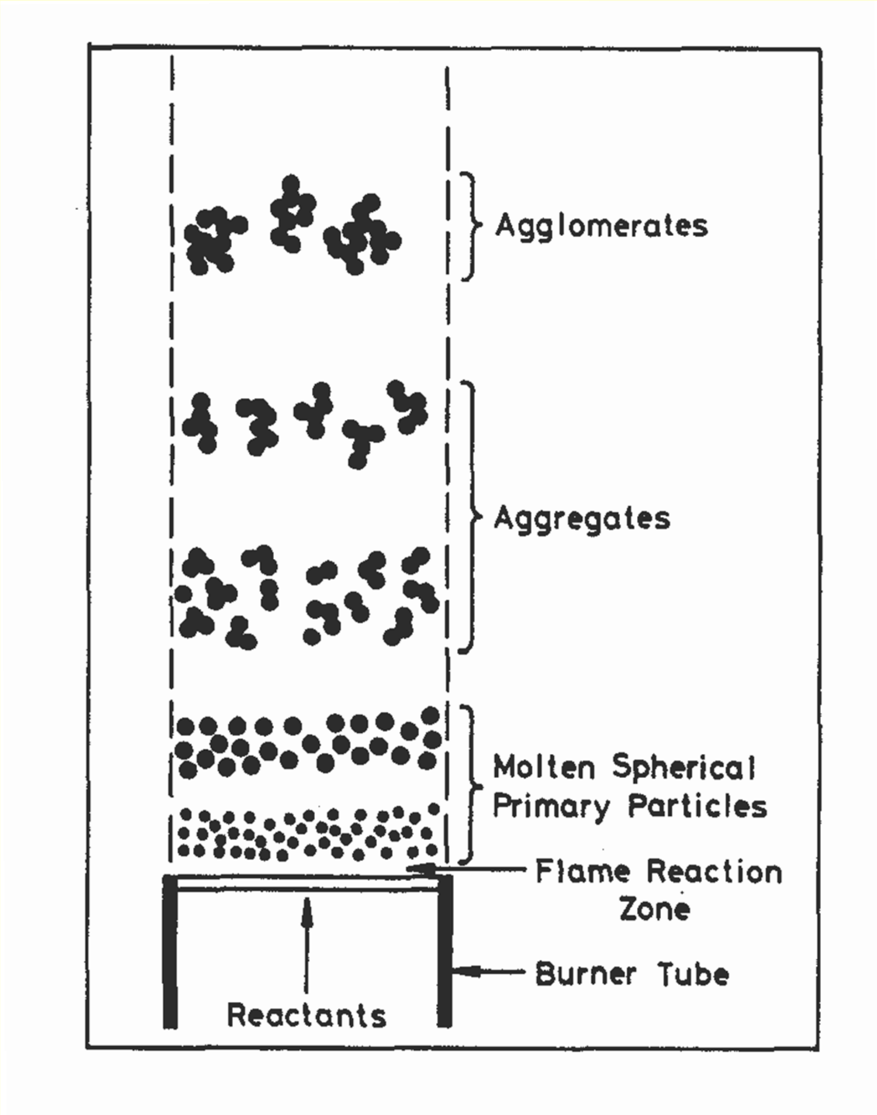

$SiCl_4 + H_2O \rightarrow OSiCl_2 + 2\ HCl$

$OSiCl_2 + H_2O \rightarrow SiClOOH + HCl$

$SiClOOH \rightarrow SiO_2 + HCl$

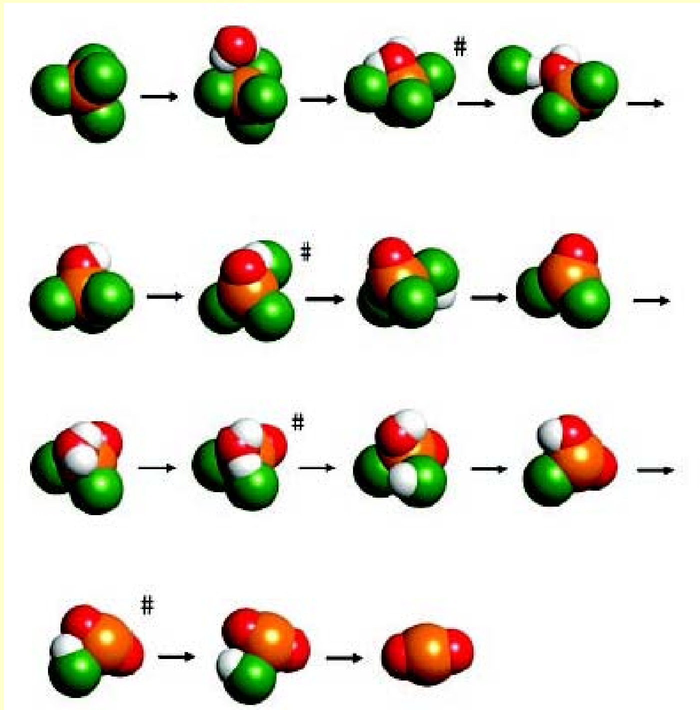

Gas Phase Reactions

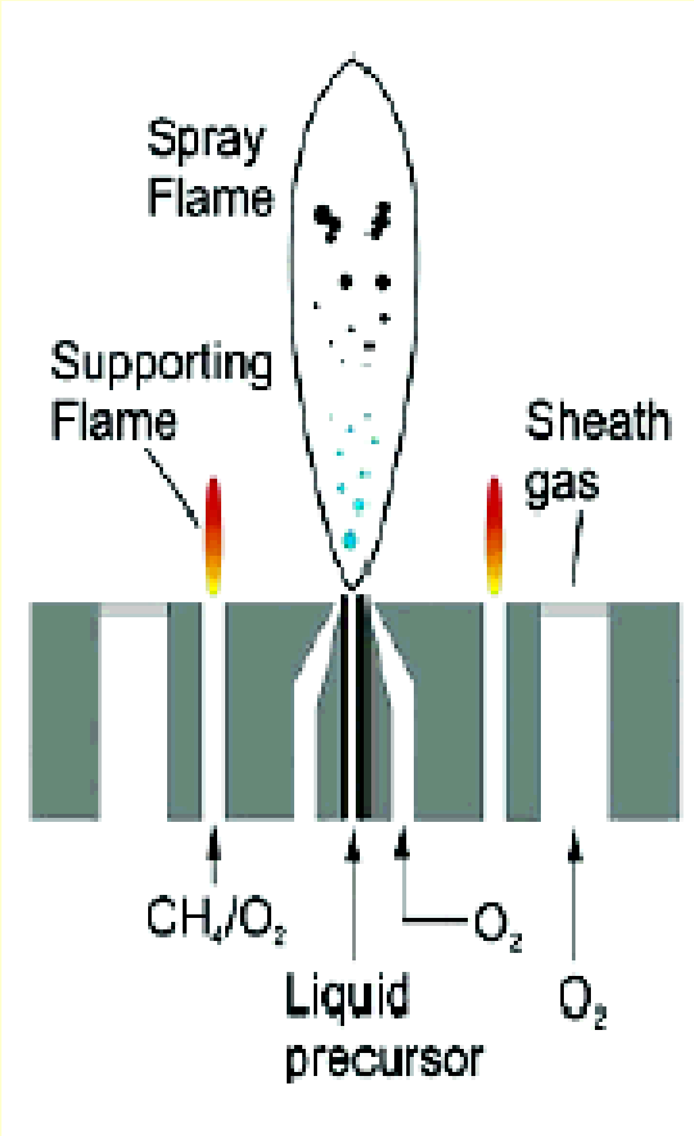

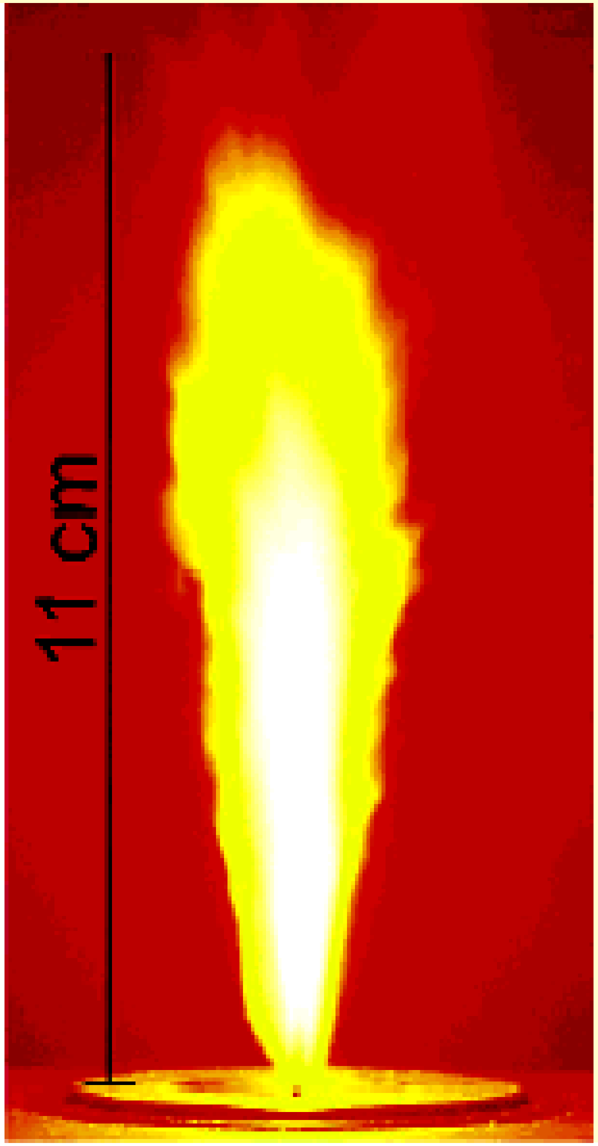

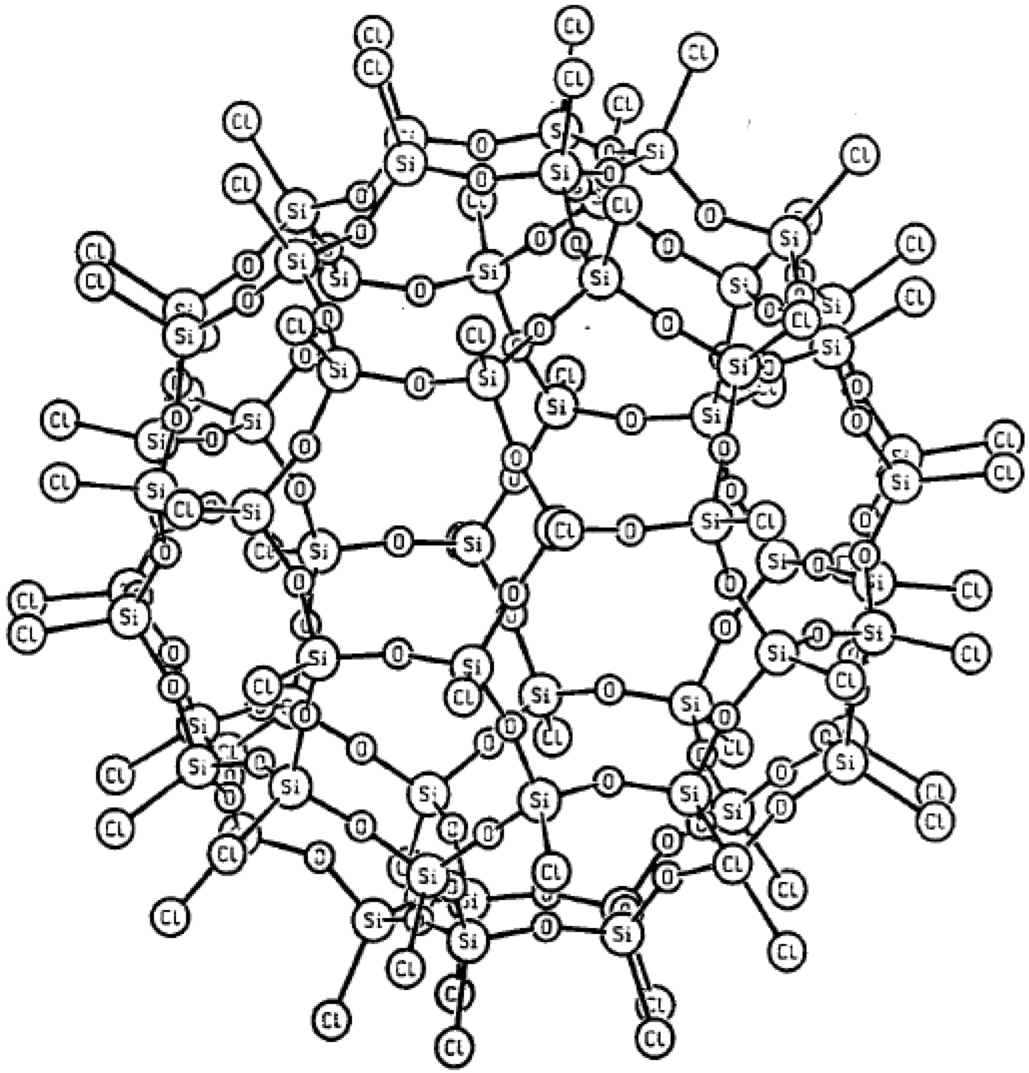

$Si_{60}O_{90}Cl_{60}$ (I_h)

Y_2O_3 Particles by Flame Aerosol Process

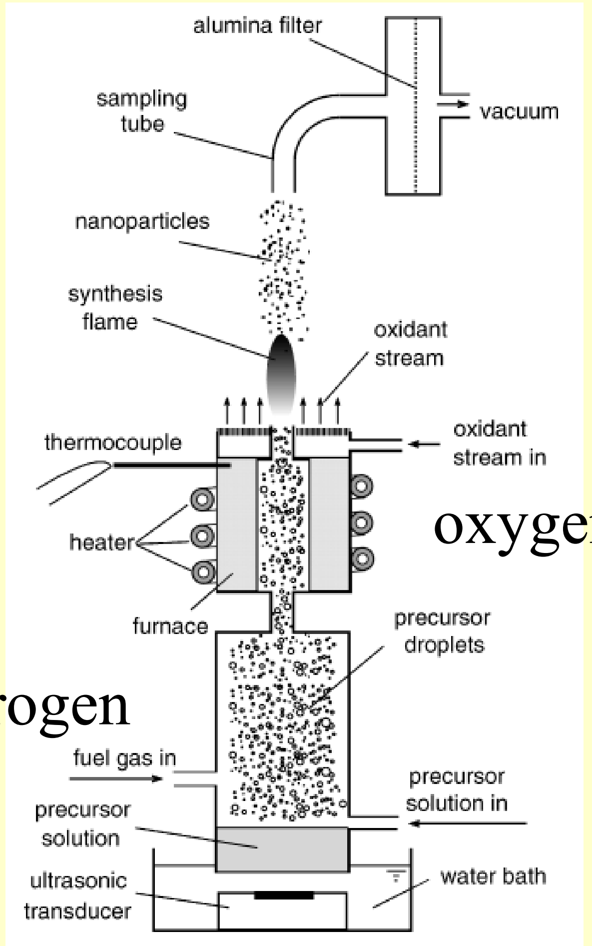

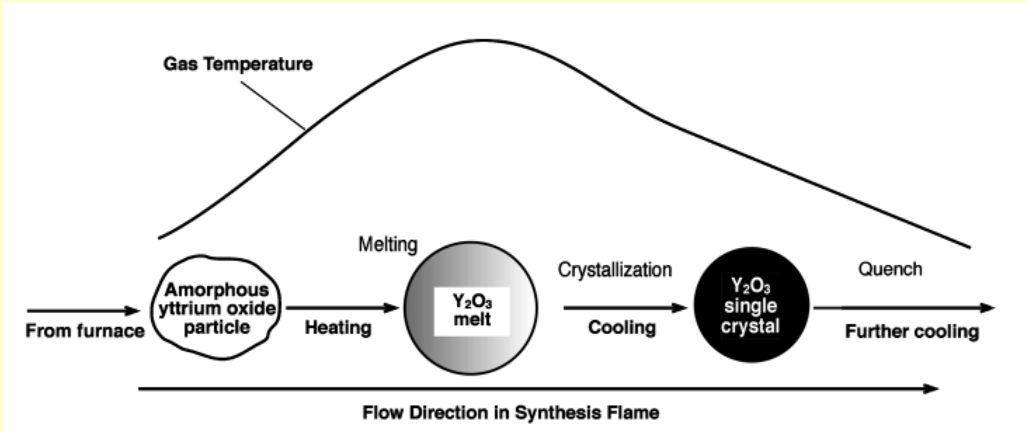

oxygen

hydrogen

$Y(NO_3)_3$

Particle Size Control

Particle size control by precursor concentration

Higher concentration = larger size

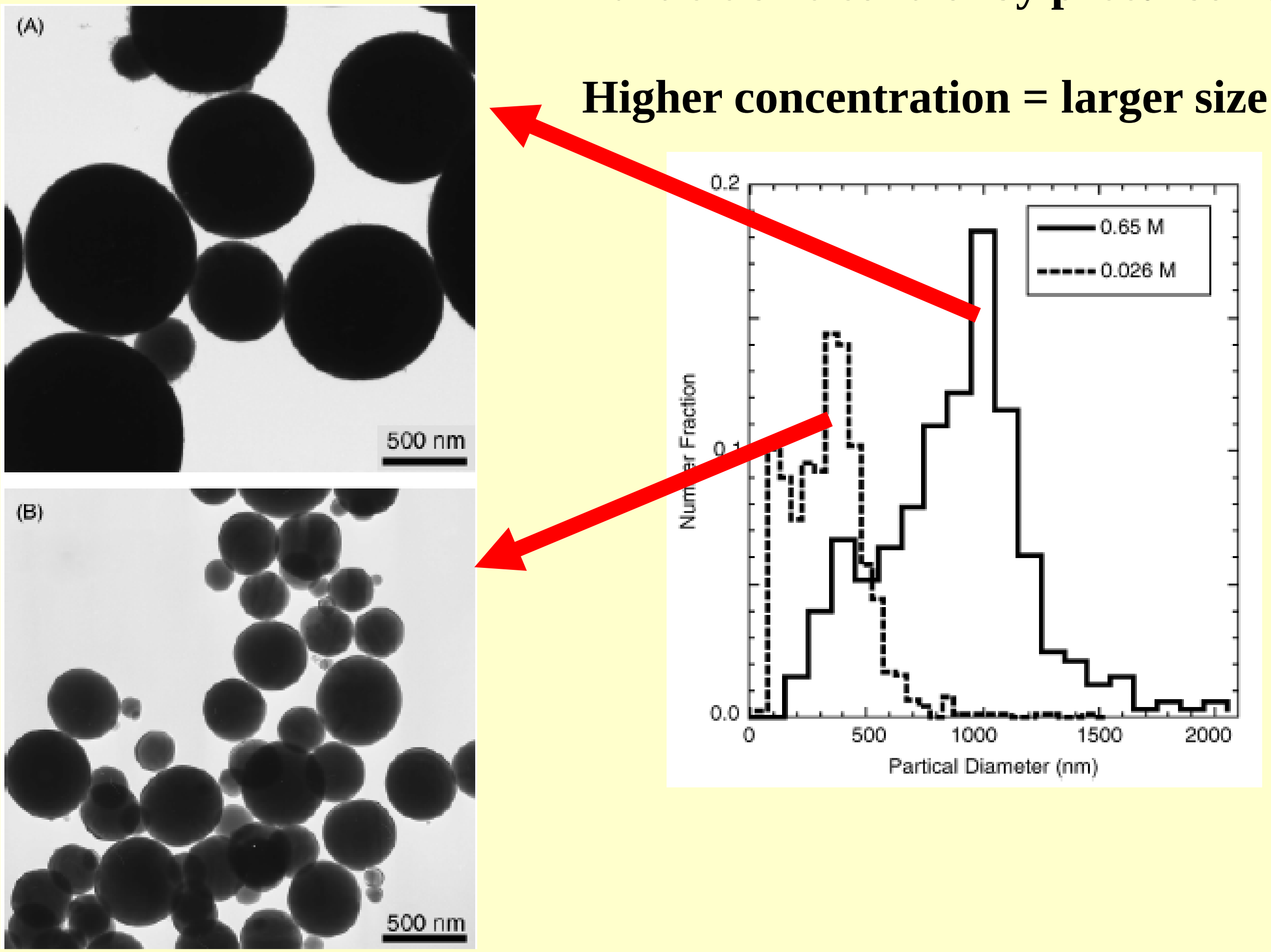

Gas Phase Reactions

Calcium phosphate nanoparticles Ca/P molar ratios 1.43 to 1.67

synthesized by simultaneous combustion of
$Ca(OAc)_2 + OP(O^nBu)_3$ in a flame spray reactor

Fluoro-apatite and zinc or magnesium doped calcium phosphates
adding trifluoroacetic acid or metal carboxylates into the fuel.

Nanoparticle morphology

At a molar ratio of Ca/P < 1.5 promoted the formation of dicalcium pyrophosphate ($Ca_2P_2O_7$).

Phase pure tricalcium phosphate TCP - $Ca_3(PO_4)_2$
obtained with a precursor Ca/P ratio of 1.52 after subsequent calcination at 900 °C

micropores and the facile substitution of both anions and cations
possible application as a biomaterial.

Spray Pyrolysis

tubular furnace reactor

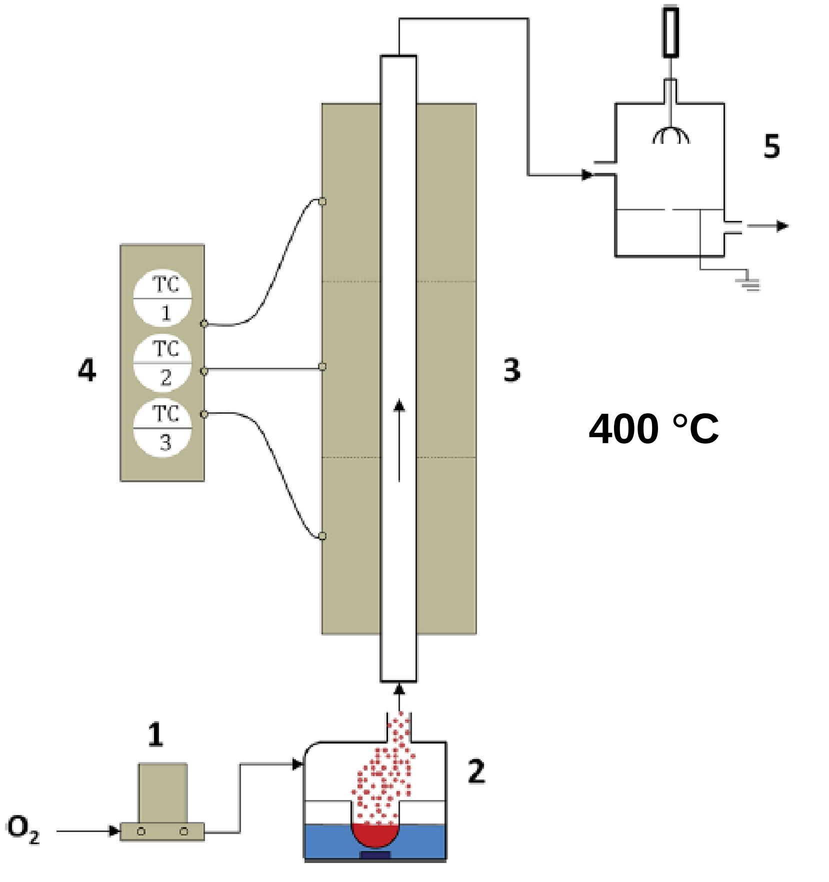

(1) mass flow controller – O_2 1 L/min
(2) ultrasonic nebulizer – aqueous solution
2 $Co(OAc)_2$: 1 $Ni(OAc)_2$
(3) 3-zone heater - 400 °C
(4) temperature controller
(5) electrostatic precipitator

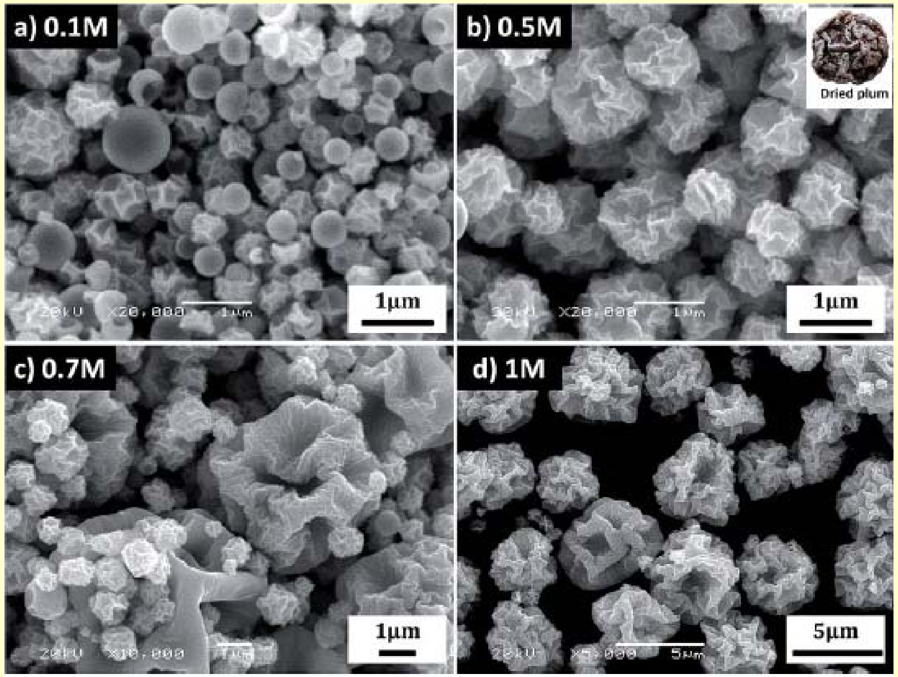

SEM micrographs of $NiCo_2O_4$ particles obtained from different concentrations of $Co(OAc)_2$ and $Ni(OAc)_2$ precursor solutions – Lower concentration reduces particle size

Morphology Control

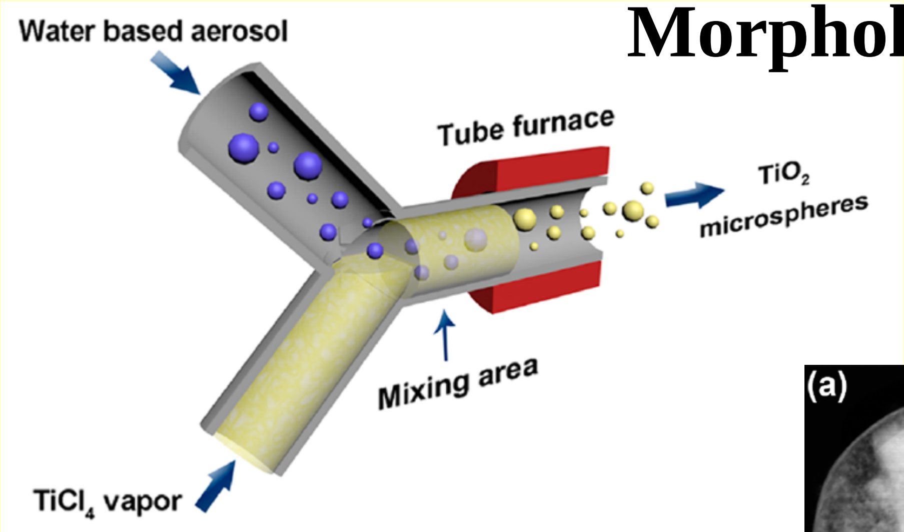

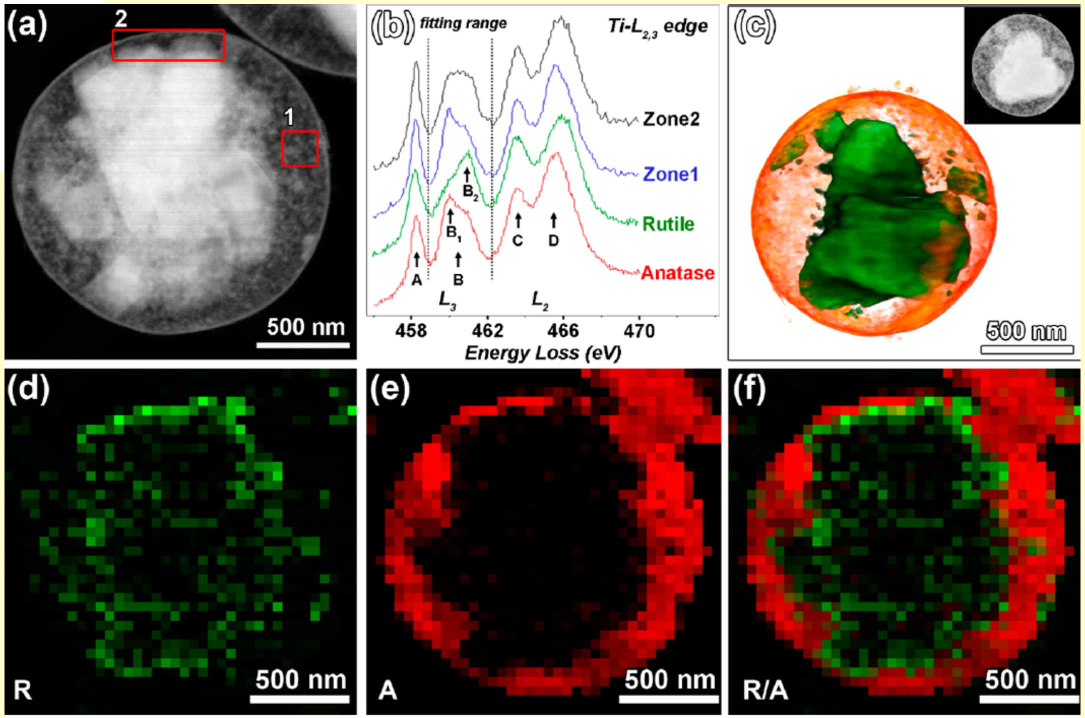

(a) HAADF-STEM of a rutile@anatase core@shell microsphere; (b) titanium L2,3 core-loss EELS spectra acquired from the indicated areas compared to reference TiO2 polymorphs [rutile (green) and anatase (red)] (d−f) EELS maps: (d) rutile (green), (e) anatase (red), and (f) rutile and anatase overlaid color map. (c) 3D tomographic reconstruction of another typical rutile@anatase core−shell microsphere, together with the corresponding HAADF-STEM image (inset).

Gas Phase Reactions

High-power CO_2 lasers

$$3\,SiH_4 + 4\,NH_3 \longrightarrow Si_3N_4 + 12\,H_2$$

$$HN(SiMe_3)_2 + NH_3 \longrightarrow Si_3N_4 + SiC$$

DC-Ar Plasma

$$TiCl_4 + NH_3 \xrightarrow{1300\ K} TiN + HCl$$

Tarnishing of Metal Surfaces

oxide, hydroxide layers

Arc

$$\text{Graphite} \longrightarrow C_{60}$$

Vapor Phase Transport Syntheses

Sealed glass tube reactors
Solid reactant(s) A + gaseous transporting agent B
Temperature gradient furnace $\Delta T \sim 50\ ^{o}C$

Equilibrium established A(s) + B(g) $\leftrightarrow$ AB(g)
Equilibrium constant K
A + B react at T_2
Gaseous transport by AB(g)
AB(g) decomposes back to A(s) at T_1, crystals of pure A
Temperature dependent K
Equilibrium concentration of AB(g) changes with T
Different at T_2 and T_1
Concentration gradient of AB(g) = driving force for gaseous diffusion

traces of a transporting agent B (e.g. I_2)

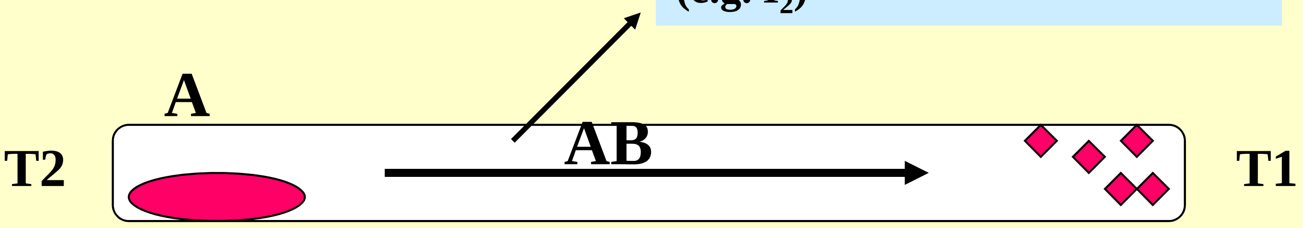

Vapor Phase Transport Syntheses

Whether T1 < T2 or T1 > T2 depends on the thermochemical balance of the reaction !
Transport can proceed from <u>higher to lower</u> or from <u>lower to higher</u> temperature

Example: $Pt(s) + O_2(g) \leftrightarrow PtO_2(g)$

Endothermic reaction, PtO_2 forms at hot end, diffuses to cool end, deposits well formed Pt crystals, observed in furnaces containing Pt heating elements

Chemical vapor transport, $T_2 > T_1$, provides concentration gradient and thermodynamic driving force for gaseous diffusion of vapor phase transport agent AB(g)

Uses of VPT

- **synthesis of new solid state materials**
- **growth of single crystals**
- **purification of solids**

Vapor Phase Transport Syntheses

Thermodynamics of VPT

Reversible equilibrium needed: $\Delta G^o = -RT\ln K_{equ} = \Delta H^o - T\Delta S^o$

☟ **Exothermic $\Delta H^o < 0$**
Smaller T implies larger K_{equ}
AB forms at cooler end, decomposes at hotter end of reactor

$W + 3Cl_2 \leftrightarrow WCl_6$ 400/1400 (exo)
$Ni + 4CO \leftrightarrow Ni(CO)_4$ 50/190 (exo)

☟ **Endothermic $\Delta H^o > 0$**
Larger T implies larger K_{equ}
AB forms at hotter end, decomposes at cooler end of reactor

$2Al + AlCl_3 \leftrightarrow 3\,AlCl$ 1000/600 (endo)
$4Al + Al_2S_3 \leftrightarrow 3Al_2S$ 1000/900 (endo)

van't Hoff equation

$$\ln K_2 - \ln K_1 = \ln \frac{K_2}{K_1} = \frac{\Delta H^0}{R}\left(\frac{1}{T_1} - \frac{1}{T_2}\right)$$

Vapor Phase Transport Syntheses

Estimation of the thermochemical balance (ΔH) of a transport reaction:

e.g.:

$$ZnS_{(s)} + I_{2(gas)} \leftrightarrow ZnI_{2(gas)} + S_{(g)} \quad \Delta H = ??$$

$$Zn_{(s)} + I_{2(g)} \leftrightarrow ZnI_{2(gas)} \quad \Delta H = -88 \text{ kJ mol}^{-1}$$

$$ZnS_{(s)} \leftrightarrow Zn_{(s)} + S_{(g)} \quad \Delta H = +201 \text{ kJ mol}^{-1}$$

$$\sum \quad ZnS_{(s)} + I_{2(gas)} \leftrightarrow ZnI_{2(gas)} + S_{(g)} \quad \Delta H = +113 \text{ kJ mol}^{-1}$$

endothermic reaction, transport from <u>hot to cold</u>!

Applications of VPT Methods

💣 Purification of Metals: Van Arkel Method

$Cr(s) + I_2(g)\ (T_2) \leftrightarrow (T_1)\ CrI_2(g)$

Exothermic, $CrI_2(g)$ forms at T_1, pure Cr(s) deposited at T_2
Useful for Ti, Hf, V, Nb, Cu, Ta, Fe, Th
Removes metals from carbide, nitride, oxide impurities

$Ti + 2I_2 \leftrightarrow TiI_4 \quad \Delta H = -376\ kJ\ mol^{-1}$
exothermic: transport from <u>cold to hot</u>

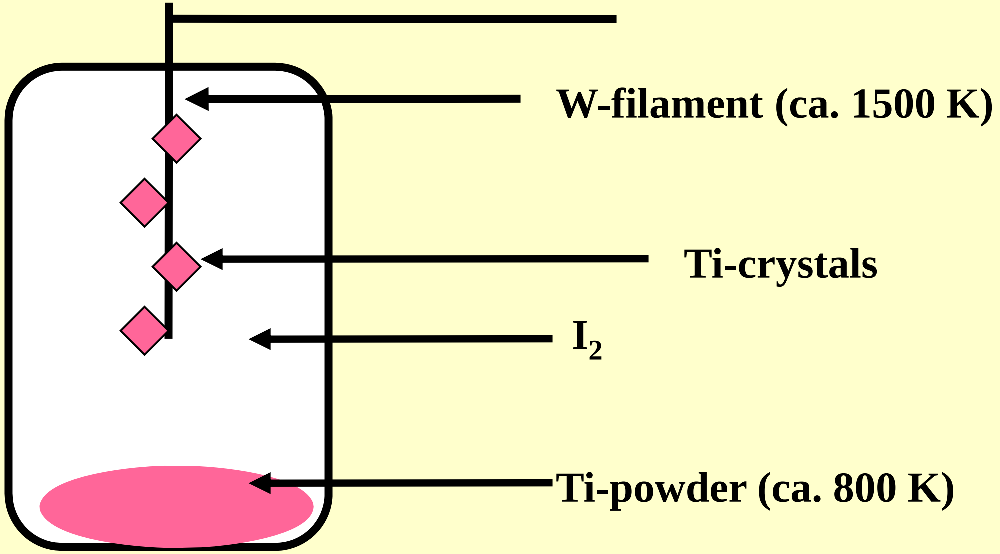

Applications of VPT Methods

💣 **Double Transport Involving Opposing Exothermic-Endothermic Reactions**

Endothermic:
$WO_2(s) + I_2(g)$ **(T_1 800°C) ↔ (T_2 1000°C)** $WO_2I_2(g)$

Exothermic:
$W(s) + 2H_2O(g) + 3I_2(g)$ **(T_2 1000°C) ↔ (T_1 800°C)** $WO_2I_2(g) + 4HI(g)$

The antithetical nature of these two reactions allows W/WO_2 mixtures to be separated at different ends of the gradient reactor using H_2O/I_2 as the transporting VP reagents

Applications of VPT Methods

💣 Vapor Phase Transport for Synthesis

$A(s) + B(g)\ (T_1) \leftrightarrow (T_2)\ AB(g)$
$AB(g) + C(s)\ (T_2) \leftrightarrow (T_1)\ AC(s) + B(g)$

Concept: couple VPT with subsequent reaction to give overall reaction:

$A(s) + C(s)\ (T_2) \leftrightarrow (T_1)\ AC(s)$

Examples:

Direct reaction sluggish even at high T

$SnO_2(s) + 2CaO(s) \rightarrow Ca_2SnO_4(s)$

Useful phosphor, greatly speeded up with CO as VPT agent:

$SnO_2(s) + CO(g) \leftrightarrow SnO(g) + CO_2(g)$
$SnO(g) + CO_2(g) + 2CaO(s) \leftrightarrow Ca_2SnO_4(s) + CO(g)$

Applications of VPT Methods

Direct Reaction:

$Cr_2O_3(s) + NiO(s) \rightarrow NiCr_2O_4(s)$ Greatly enhanced rate with O_2

$Cr_2O_3(s) + 3/2O_2 \leftrightarrow 2CrO_3(g)$
$2CrO_3(g) + NiO(s) \leftrightarrow NiCr_2O_4(s) + 3/2O_2(g)$

Overcoming Passivation Through VPT

$Al(s) + 3S(s) \rightarrow Al_2S_3(s)$ passivating skin stops reaction

In presence of cleansing VPT agent I_2:

Endothermic:
$Al_2S_3(s) + 3I_2(g)$ (T_1 700^{o}C) $\leftrightarrow$ (T_2 800^{o}C) $2AlI_3(g) + 3/2S_2(g)$

Applications of VPT Methods

💣 **Vapor Phase Transport for Synthesis**

$Zn(s) + S(s) \rightarrow ZnS(s)$
passivation prevents reaction to completion

Endothermic:
$ZnS(s) + I_2(g)\ (T_1\ 800^oC) \leftrightarrow (T_2\ 900^oC)\ ZnI_2(g) + 1/2S_2(g)$

VPT Synthesis of $ZnWO_4$:
A Real Phosphor Host Crystal for Ag^+, Cu^+, Mn^{2+}

$WO_3(s) + 2Cl_2(g)\ (T_1\ 980^oC) \leftrightarrow (T_2\ 1060^oC)\ WO_2Cl_2(g) + Cl_2O(g)$

$WO_2Cl_2(g) + Cl_2O(g) + ZnO(s)\ (T_2\ 1060^oC) \leftrightarrow ZnWO_4(s) + Cl_2(g)$

Growing Epitaxial GaAs Films by VPT Using Convenient Starting Materials

$GaAs(s) + HCl(g) \leftrightarrow GaCl(g) + 1/2H_2(g) + 1/4As_4(g)$

$AsCl_3(g) + Ga(s) + 3/2H_2 \leftrightarrow GaAs(s) + 3HCl(g)$

Serves to establish initial equilibrium

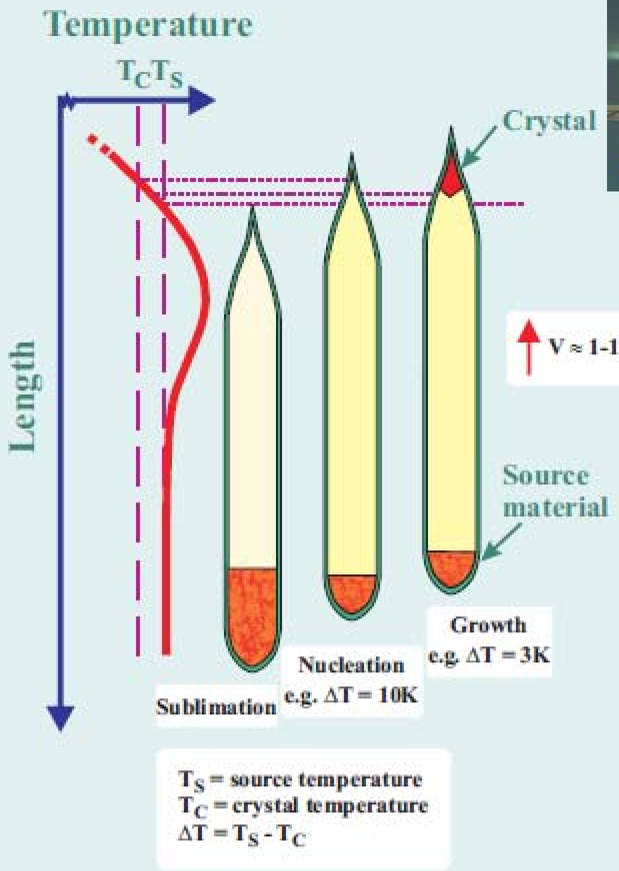

ZnSe, ZnTe, CdS

1. Purification by sublimation
2. Synthesis
3. Sublimation or chemical vapor transport

Crystals grown:

ZnO, ZnSe, ZnTe, CdS, CdSe, Ag_2S, CuCl, CuBr, CuI, AgI, TiO_2, C_{60}, C_{70}, Zn, Cd, Mg etc.

KBr GeS TlBr

A view of vapor growth equipment

Laser-induced homogeneous pyrolysis, LIHP

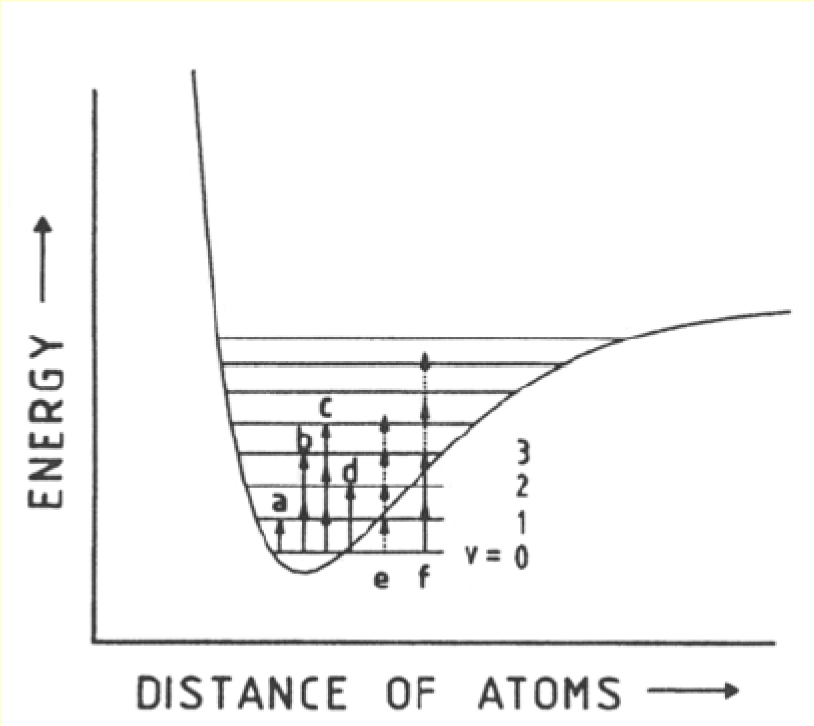

$C_2H_4 + h\nu \rightarrow C_2H_4^*$

Excitation energy transferred to vibrational-translational modes

⇒ T increases

laser wavelength
$10.60 \pm 0.05\ \mu m$

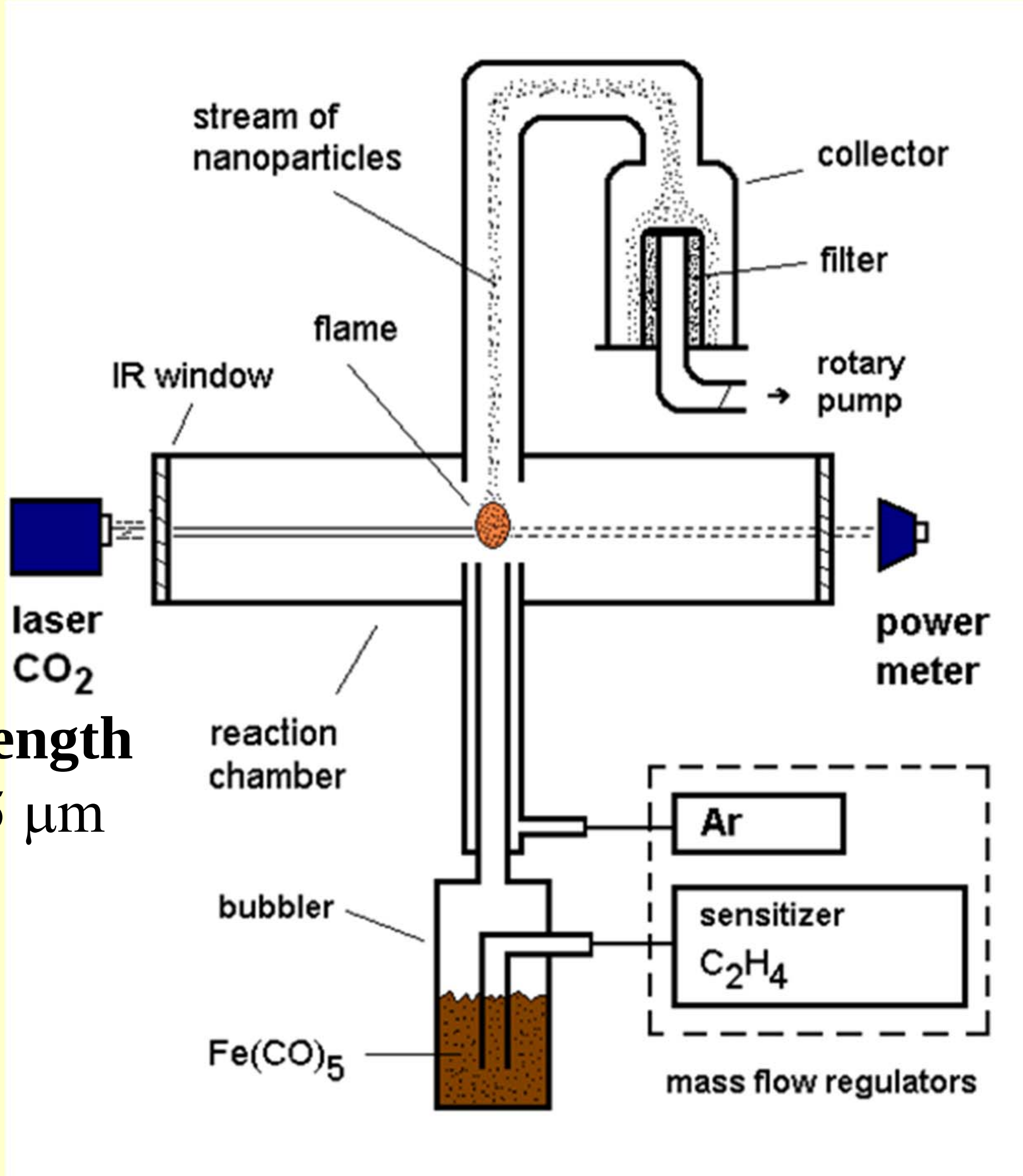

Sensitizer

SF_6
948 cm^{-1}

Isopropanol
958 cm^{-1}

Reaction Zone

Overlap between
the vertical reactant gas stream
and the horizontal laser beam

away from the chamber walls

nucleation of nanoparticles
less contamination
narrow size distribution

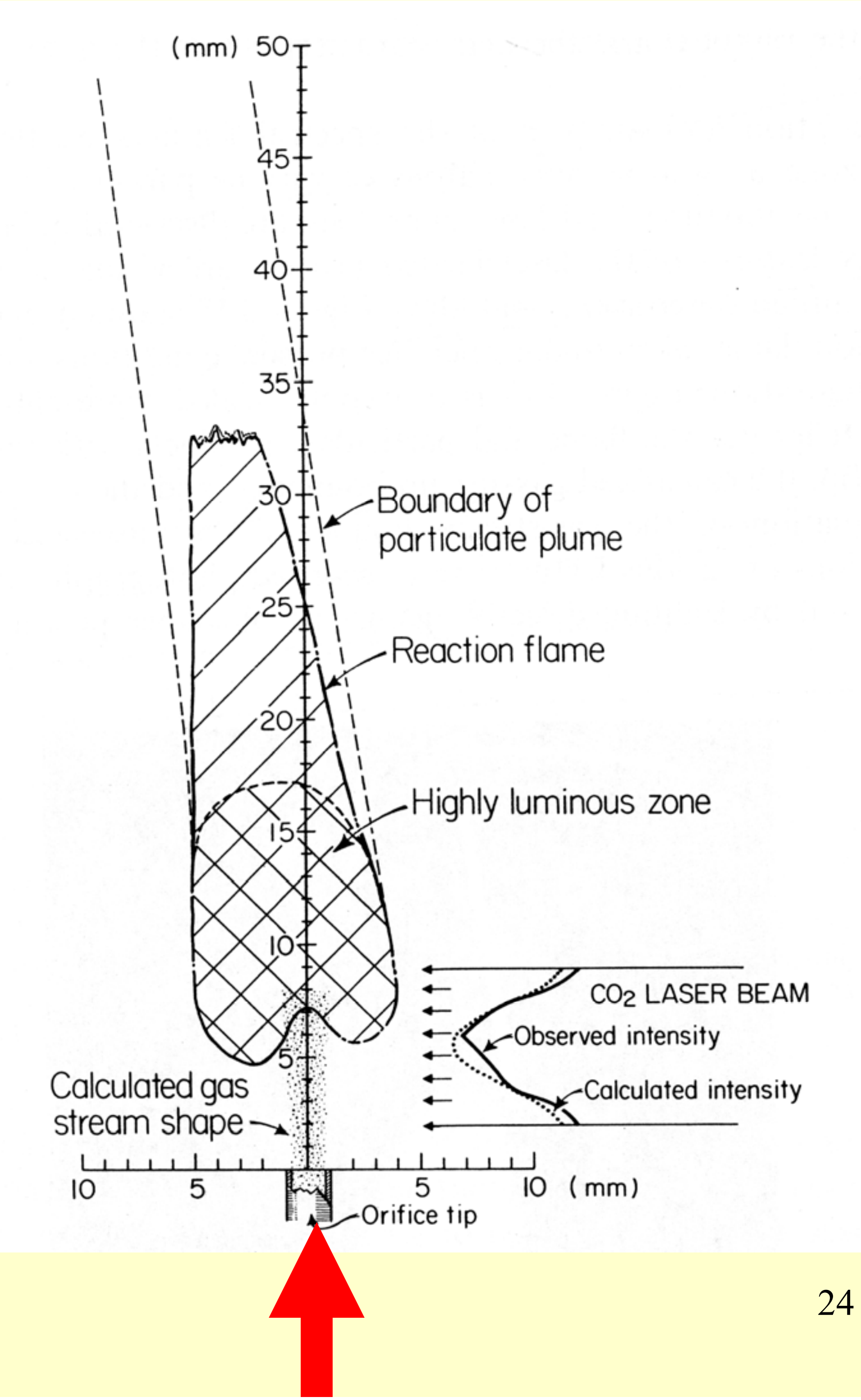

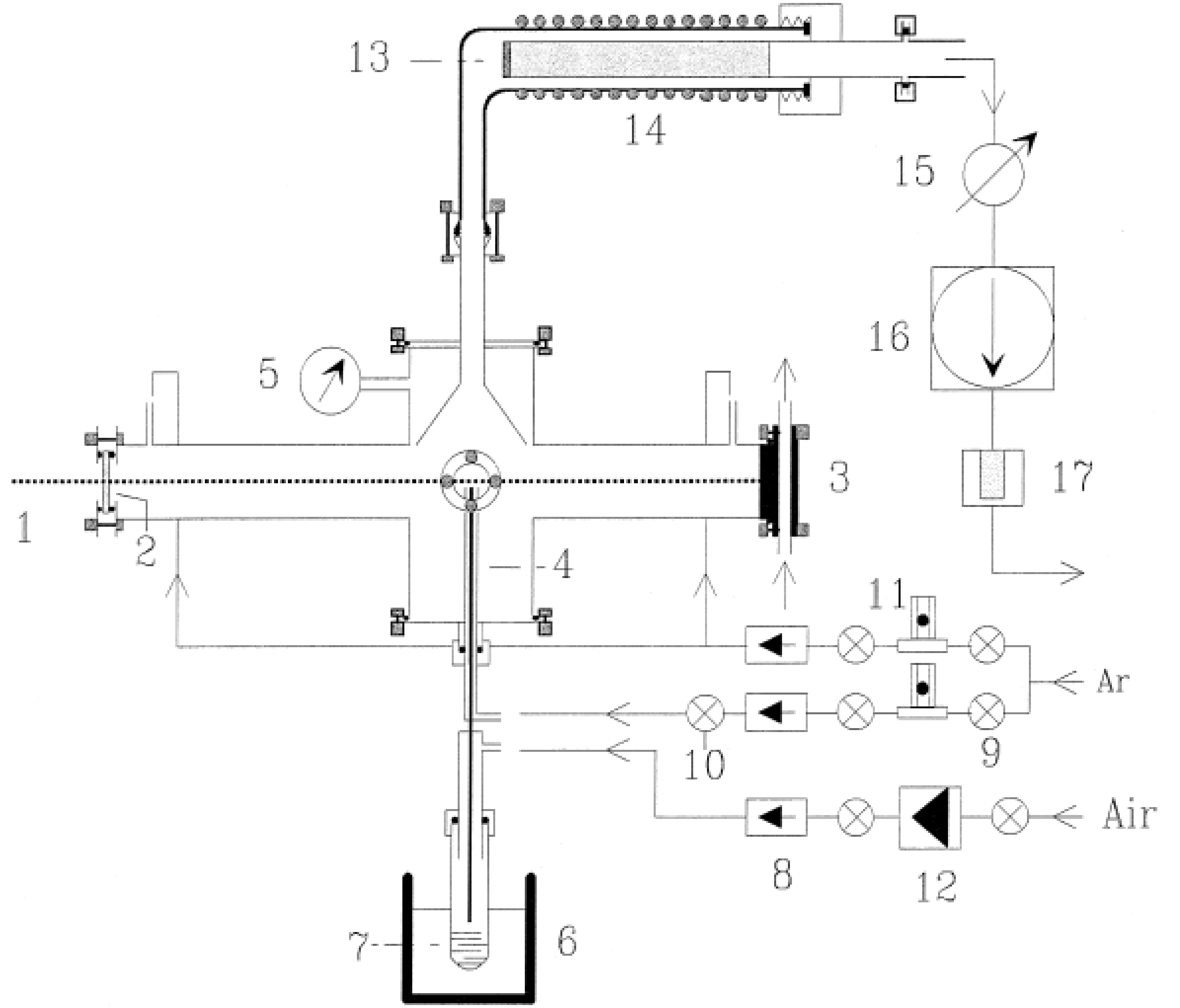

Fig. 1. CO_2 laser pyrolysis system. (1) Laser beam, (2) ZnSe window, (3) water refrigerated aluminium target, (4) nozzle, (5) pressure gauge, (6) ultrasonic bath, (7) 30% iron pentacarbonyl solution in isopropanol, (8) not return valve, (9) ball valve, (10) three ways ball valve, (11) argon rotameter, (12) massic controller of air flux, (13) stainless steel filter to collect the produced powders, (14) heating resistance, (15) pressure controller valve, (16) rotary vacuum pump, (17) filter to capture oil mist.

Iron-oxide Nanoparticles by Laser-induced Pyrolysis

$$2\,Fe(CO)_5 + 3\,N_2O \rightarrow Fe_2O_3 + 10\,CO + 3\,N_2$$

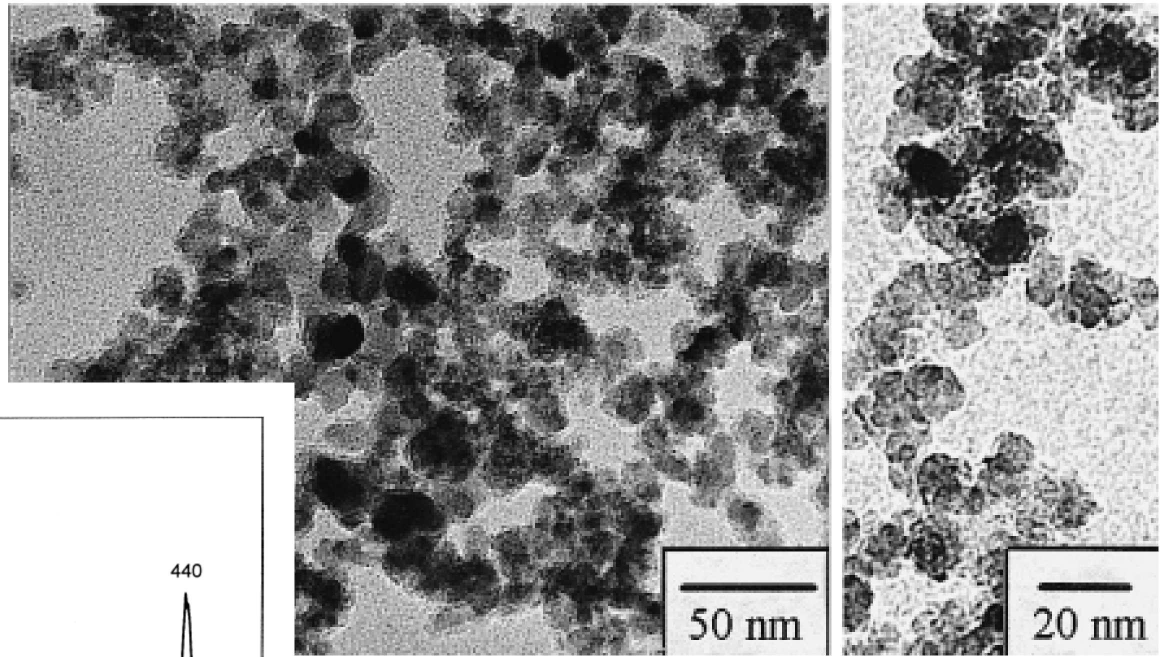

. TEM micrographs of the synthesised γ-Fe_2O_3 particles.